International Journal of Bio-Inorganic Hybrid Nanomaterials

In vitro Investigation of Polymer Coated Magnesium Incorporated by Mesoporous Silica Nanocontainers

Mahdi Yeganeh[1*], Mohsen Saremi[2]

[1] *Ph.D., Corrosion Laboratory, School of Metallurgy & Materials Engineering, University College of Engineering, University of Tehran, North Kargar, Tehran, P.O. Box 11365-4563, Iran*

[2] *Professor, Corrosion Laboratory, School of Metallurgy & Materials Engineering, University College of Engineering, University of Tehran, North Kargar, Tehran, P.O. Box 11365-4563, Iran*

ABSTRACT

The idea of smart corrosion inhibition is basis on either inhibitor consumption where it is needed or reducing harmful matrix interaction with it. In addition, applying corrosion inhibitor in a coating causes many problems such as loss of inhibition capability, coating degradation, or both. A useful technique to overcome this problem is applying of inert host systems of nanometer dimensions as nanocontainers, which is loaded by corrosion inhibitors. In the present study, mesoporous silica nanocontainers with and without inhibitor (fluoride) were dispersed in the Alkyd coatings to improve corrosion resistance of Mg metal. Then, corrosion behavior of these coatings was studied in comparison with Mg in the NaCl solution. Electrochemical tests showed that theses coatings could protect the surface from chloride solution. In addition, fluoride release from mesoporous silica nanocontainers causes MgF_2 formation in the interface, as an inhibitive compound. Furthermore, the corrosion mechanism of Mg in the chloride media was attributed to the formation of MgH_2 and $Mg(OH)_2$.

Keyword: Magnesium; Polymer Coating; EIS; Mesoporous silica; Corrosion.

1. INTRODUCTION

Magnesium is the lightest structural metals and its alloys have quite special properties leading to specific applications in automotive, aerospace, and other industries [1, 2]. Unfortunately, pure magnesium and its alloys corrode too quickly at the physiological pH (7.2-7.4) as well as in physiological media containing high concentrations of chloride ions, thereby losing mechanical integrity before the tissues have sufficient time to heal. Besides, during the corrosion process, release of hydrogen gas may be too fast to be endured by the host tissues [3].

In general, there are a few approaches to improve corrosion resistance of magnesium including changing in composition of alloy and surface treatment. Various surface treatment techniques have been used to enhance the corrosion resistance of magnesium including physical vapor deposition [4, 5], electroless plating [6, 7], plasma electrolytic oxidation [8, 9], chemical conversion treatments [10-12], sol-gel coatings [13-15], calcium phosphate coatings [16, 17], hydroxyapatite

Int. J. Bio-Inorg. Hybr. Nanomater., Vol. 3, No. 3 (2014), 135-142

Yeganeh M & Saremi M

coatings [18-20], and polymer coatings [21-23]. On the other hand, some organic coatings which can apply on the Mg alloys may endure corrosion and do not possess good properties. One of the main routes to improve corrosion resistance of polymer coating in corrosive media is to incorporate inert particles into their structures.

In this study, the mesoporous silica powders were applied as incorporating particles to serve as corrosion inhibitor hosts. This material has a hexagonal packing of uniform cylindrical pores with the diameter in the range of 2-50 nm, high surface area (500-1500 $m^2.g^{-1}$), large pore volume (1 $cm^3.g^{-1}$), high chemical and thermal stability, and easy functionalization [24, 25]. Furthermore, these materials have found to be biocompatible for different application such as drug delivery. Therefore, the incorporation of mesoporous materials in the polymer matrix is not harmful for internal tissues [26].

The main purpose of this work is to study corrosion behavior of Alkyd coating impregnated by mesoporous silica nanocontainers coated on Mg. In this regard, we applied air dried Alkyd resin with Soya solvent as a coating on Mg. Fluoride ion corrosion inhibitor was loaded in the functionalized mesoporous silica. Then, these loaded mesoporous silica powders were dispersed in the Alkyd coatings. Next, these composite coatings were characterized in the NaCl solutions. By immersing Alkyd/inhibitor loaded mesoporous silica in the corrosive media, it is expected that the corrosion inhibitors release and subsequently hinder the corrosion process. Besides, these powders can serve as a barrier delaying the movement of corrosive species to the metal surface. To prove effectiveness of the inhibitor containing coatings, functionalized mesoporous silica without any adsorbed inhibitor was loaded in the Alkyd coatings and the corrosion properties were compared with the case of using adsorbed inhibitor and bare Mg.

2. EXPERIMENTAL

Materials and Methods

Mesoporous silica powders were synthesized by mixing surfactant molecules such as cetyltrimethylammoniumbromide (CTAB) and a silica precursor (tetraethylorthosilicate, TEOS) as reported in literatures [24]. Then, the initial mesoporous silica was functionalized by silane group (1-(2-aminoethyl)-3aminopropyltrimethoxysilane) in the toluene and heated up to 400 K in inert ambient for 16 h. The powders were filtered and washed by ethanol. In the next step, Fe^{3+} ($FeCl_3$) was incorporated in the functionalized mesoporous silica in the propanol solution at ambient temperature for 6 h. The powder obtained from filtration and washing is denoted as MS. Finally, the corrosion inhibitor (NaF) adsorption process was carried out for 24 h, following by filtering and washing by ethanol and drying. The obtained powder denoted as MSInh can be applied as corrosion inhibitor nanocontainer in the coatings. The size and morphologies of mesoporous silica powder were studied using a high resolution scanning electron microscope (FESEM Hitachi SU8040, 40 kV) and a transmission electron microscope (TEM Tecnai G2 F30 at 300 kV). The specific surface area, average pore diameter, and pore volume were obtained from N_2 adsorption–desorption isotherms (BELSORP mini-II). The specific surface area was calculated using the adsorption data in the low pressure range by the Brunauer–Emmett–Teller (BET) method. The average pore diameter and the pore volume were determined from N_2 desorption branch of the nitrogen isotherms using the Barret–Joyner–Halenda (BJH) method.

The Alkyd resin was mixed with reactive diluent. Then, mesoporous silica powders (with or without inhibitor) were added to the mixture (1 wt.%). The suspension was stirred at 1200 rpm for 2 h. The mixtures were then sonicated for 1 h and mixed with hardener in 10:1 ratio. The synthesized composites were applied on Mg plates and cured at room temperature for two days.

Corrosion properties of Mg, Alkyd/MS, and Alkyd/MSInh coatings in the NaCl solution were investigated at various times (1 h, 5 h, 1 day, and 1 week) by electrochemical tests. The electrochemical measurements were carried out in a classical electrochemical cell with an Mg and Mg plates coated by Alkyd/MS and Alkyd/MSInh as working electrode with an exposed area of 1 cm^2. A platinum plate was used as the counter electrode, while a saturated calomel electrode (SCE) was taken as a reference electrode. All OCP tests were performed on

Yeganeh M & Saremi M

Int. J. Bio-Inorg. Hybr. Nanomater., Vol. 3, No. 3 (2014), 135-142

an EG&G potentiostat-galvanostat 273A model equipment controlled by software M352. The AC amplitude was 5 mV and the frequency was set in the range of 100 kHz to 10 MHz using a 1260 Solarton frequency response analyzer (FRA). Surface morphology after corrosion was examined using the high resolution scanning electron microscope (FESEM ZEISS) and optical microscope (Gippon Inc.)

3. RESULTS AND DISSCUSION

3.1. *Mesoporous silica analysis*

Figure 1a-d illustrates micrograph and schematic figure of mesoporous silica. Figure 1a shows morphology of mesoporous silica, where diameter of each mesoporous silica tube varies from 50 to 300 nm, while their length was in micrometer range. Also, Figure 1b shows TEM micrograph of mesoporous silica with hexagonal pores. The average diameter of the pores obtained by TEM was about 4 nm. Figure 1c demonstrates schematic view of hexagonal mesoporous structures with Si-OH configuration in the pores (Figure 1d).

Specific surface area, pore volume, and average pore diameter of the mesoporous silica was obtained 776.2 $m^2.g^{-1}$, 0.84 $cm^3.g^{-1}$, and 4.23 nm, respectively by N_2 adsorption/desorption technique. These parameters for MSInh were gained 540.1 $m^2.g^{-1}$, 0.55 $cm^3.g^{-1}$, and 3.5 nm, respectively. Specific surface area, pore volume, and pore diameter size decreased after functionalization and adsorption of fluoride ions on the surface of mesoporous silica.
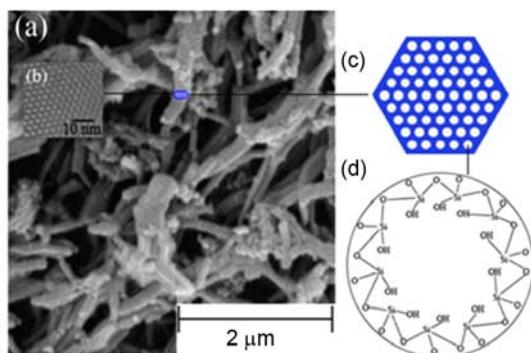
Figure 1: *(a) SEM and (b) TEM micrograph of mesoporous silica, (c) schematic form of hexagonal mesoporous structures, and (d) Si-OH configuration in the pores.*

3.2. *Corrosion investigation of alkyd coatings*

Figure 2a-b shows schematic Nyquist plot of Mg, Alkyd/MS and Alkyd/MSInh in the NaCl solution at the initial and final immersion times. As observed in these figures, Mg shows a capacitive loop at high frequencies followed by an inductive loop at low frequencies. There are various explanations for this inductive loop such as relaxation process of adsorbed species [27-29], pitting [30, 31], hydroxide formation [32, 33], partial protection of oxide film on the surface [34], or auto catalytic damage process of the surface film [35]. Some remarks about corrosion mechanism of Mg are presented in section 3.3.

The related Nyquist plot for coatings shows two time constant at high and low frequencies. High frequency loop is related to coating resistance, while low frequency loop shows charge transfer resistance in the Mg/polymer interface. At initial times, contribution of charge transfer is very low due to the inadequate dif-

(a)

(b)
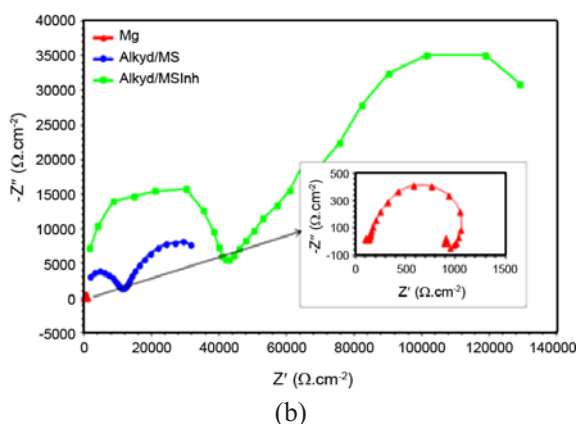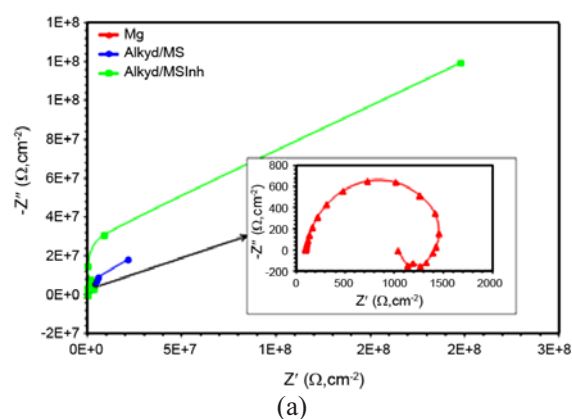
Figure 2: *Schematic Nyquist plot of Mg, Alkyd/MS and Alkyd/MSInh in the NaCl solution at the initial and final times of immersion.*

Int. J. Bio-Inorg. Hybr. Nanomater., Vol. 3, No. 3 (2014), 135-142

Yeganeh M & Saremi M
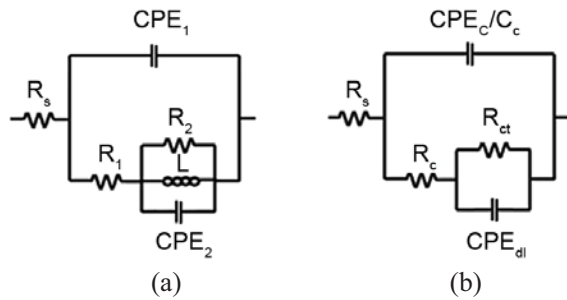
Figure 3: *Equivalent circuits for (a) Mg and (b) Alkyd coatings in the NaCl solutions.*

fusion of corroding ions to the interface. In comparison, by applying Alkyd coatings, the inductive loops disappear, which could be due to preventing corrosion and insufficient access of corrosive ions to the surface. Therefore, it could be stated that the formation of inductive loop is because of the formation of corrosion product on the surface.

Figure 3a-b shows equivalent circuits for these two Mg and Alkyd coatings, respectively. The model includes the solution resistance R_s, a series combination of resistance, R, and inductance, L, in parallel with charge transfer resistance R_{ct}, and the constant phase

element (CPE). CPE was used instead of a pure capacitance (C) accounting for a non-ideal capacitive response of the interface. The impedance of a CPE is equal to $A^{-1} (i \omega)^{-n}$, where A is the constant corresponding to the interfacial capacitance, i is the imaginary number, ω is the angular frequency, and n is an exponential factor in the range between -1 and 1. Depending on the value of n, CPE can represent resistance (n = 0, A = R), capacitance (n = 1, A = C), inductance (n = −1, A = L) or Warburg impedance (n = 0.5, A = W). Pure capacitance behavior is indicated by n = 1, while in practice n often ranges from zero to 1. Heterogeneity of the water uptake phenomenon could impose deviating from pure capacitor [36, 37].

Besides, n is associated to the degree of roughness and the geometry of the coatings [38]. R_{ct} is defined as the value corresponding to Z' when –Z" = 0, commonly obtained at intermediate frequencies, while R_P is defined as the zero frequency impedance at –Z" = 0 often assessed at f→0 [39]. Rct for this kind of plot is calculated according to fitting results. R_{ct} for Mg after corrosion for 1 h, 5 h, 1 day, and 1 week was obtained as 1310, 1270, 990, and 890 $\Omega.cm^2$, respectively.
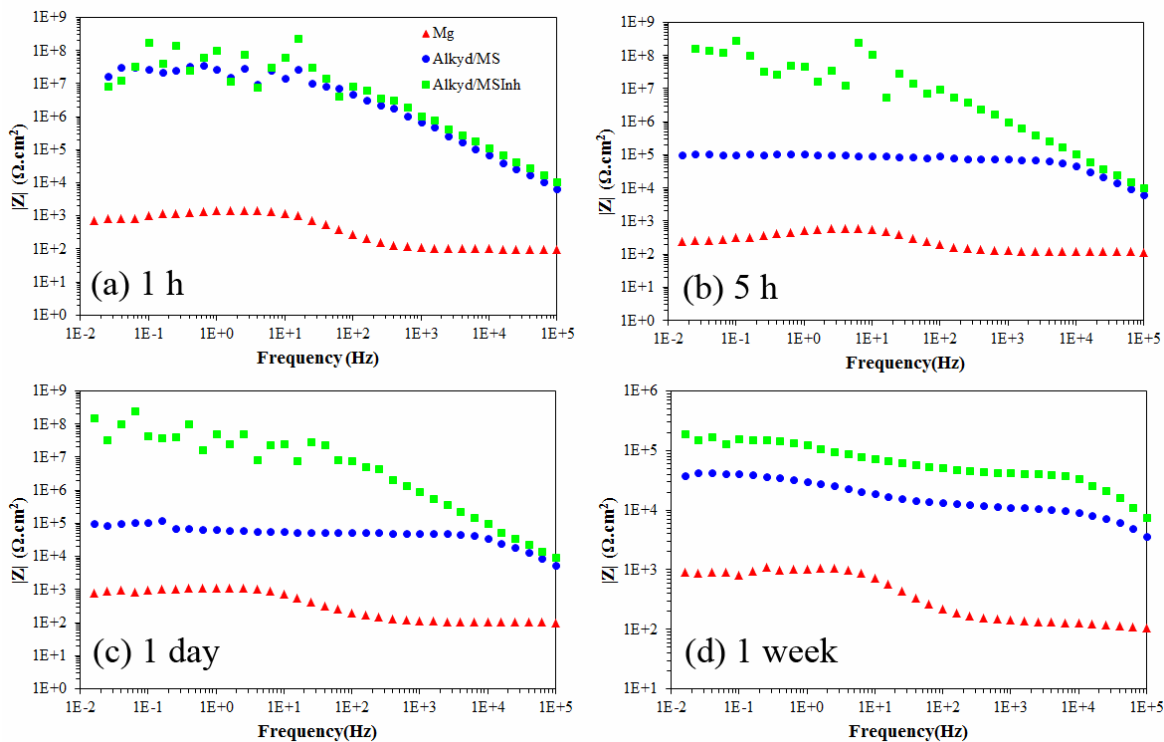
Figure 4: *Bode plots for Mg, Alkyd/MS, and Alkyd/MSInh in NaCl solution after 1 h, 5 h, 1 day, and 1 week immersion.*

Table 1: Impedance data obtained for Alkyd/MS and Alkyd/MSInh at different times in NaCl solution.

	Time	C_c(nF)	$|Z|_{0.1Hz}$(kΩ.cm^2)	θ_{10kHz}
Alkyd/MS	1 h	0.23	27949.3	84
	5 h	0.35	98.6	47.2
	1 day	0.43	106.4	39.9
	1 week	1.7	40.9	18.2
Alkyd/MSInh	1 h	0.13	176051.6	83.9
	5 h	0.15	294421	83.7
	1 day	0.16	45348.8	83
	1 week	0.46	160.3	27.5

Figure 4a-d shows Bode plots for Mg, Alkyd/MS, and Alkyd/MSInh in NaCl solution after 1 h, 5 h, 1 day, and 1 week immersion.

To determine electrochemical properties of Alkyd coatings, three different parameters C_c, $|Z|_{100}$ MHz and θ_{10} kHz were chosen [40]. The higher is the value of these parameters, the greater is the corrosion resistance. Impedance magnitude at 100 MHz ($|Z|_{100\ MHz}$) and phase angle at 10 kHz ($\theta_{10\ kHz}$) give qualitative information about corrosion protection. Once a capacitor and a resistor are parallel, phase difference between current and voltage is a criterion for current to transmission through either capacitor or resistor. The electrochemical behavior of metal-electrolyte interface is capacitive if charge transfer resistance and/ or double layer capacitance are high. In such a case, current would mostly pass through capacitor and, therefore, phase angle would be near 90°. Moreover, the electrochemical behavior of metal-electrolyte in-

terface is resistive if resistance and/or capacitance are low. Consequently, current would frequently pass through resistor; therefore, phase angle would be near zero [40]. According to Table 1, the highest value of phase angle at 10 kHz ($\theta_{10\ kHz}$) obtained for Alkyd/MS solution is about 84°.

It was shown that for intact coatings the value of θ is close to 90° [40]. Phase angle at initial times is close to each other for both Alkyd/MS and Alkyd/MSInh, implying the insufficient release of fluoride ion from MSInh. On the other hand, at the initial times corrosive ions do not have enough time to pass through polymer matrix. As time proceeds, phase angle for Alkyd/MSInh becomes greater than that of Alkyd/MS, which could be attributed to the formation of protective compounds due to fluoride release from MSInh. On the other hand, by passing time, coatings had the higher affinity to ions and became more conductive. In other words, an increase in the C_c value is attributed to the accumulation of conducting species into the porosities of the coatings.

XRD patterns after corrosion revealed that MgO (dried Mg(OH)$_2$) is the most corrosion product on the Mg surface, while trace of MgCl$_2$ is also detectable in XRD pattern (Figure 5). Coatings had more intact Mg peaks due to lower corrosion products. Besides, Alkyd/MSInh presented a peak related to MgF$_2$. It seems that the Mg(OH)$_2$ film (slightly stable in water) reacts with fluorides and develops fluoride containing Mg compounds according to Eq. 1:
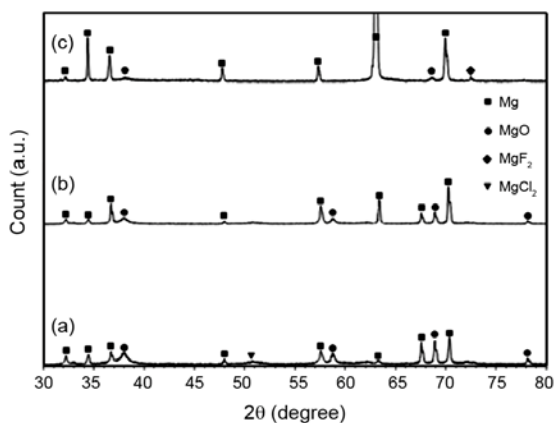
Figure 5: XRD patterns after corrosion for (a) Mg, (b) Alkyd/MS, and (c) Alkyd/MSInh.

$$\text{Mg(OH)}_2 + 2\text{F}^- \rightarrow \text{MgF}_2 + 2\text{OH}^- \tag{1}$$

Int. J. Bio-Inorg. Hybr. Nanomater., Vol. 3, No. 3 (2014), 135-142

Yeganeh M & Saremi M
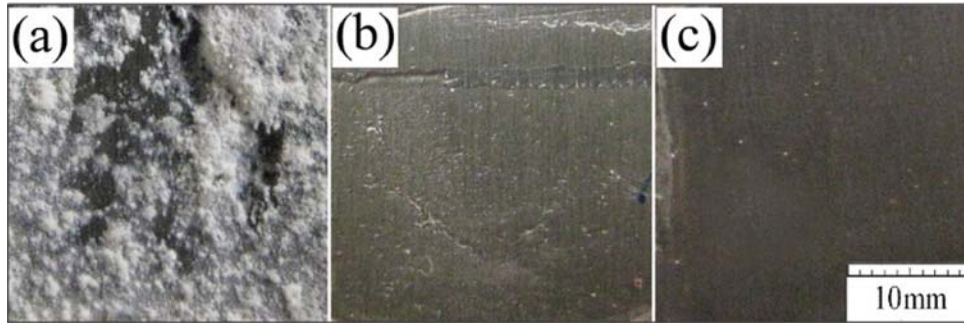
Figure 6: Surface after corrosion for (a) Mg, (b) Alkyd/MS, and (c) Alkyd/MSInh.

Figure 6a-c shows optical surface morphology after corrosion where Mg surface is highly corroded; however the mentioned two coatings show more intact surfaces. In addition, Alkyd/MSInh also had no obvious pit on its surface, while Alkyd/MS revealed some pits on its surface due to chloride attack. Development of several white spot on Alkyd/MS and Alkyd/MSInh might be attributed to corrosion production such as MgO.

3.3. Some comments about corrosion of Mg

According to Pourbaix diagram proposed by Chen et al. [41] (Figure7), it assume that in the initial times of corrosion (A: pH = 7.3, OCP = -1.5 V vs. SCE), the state of Mg is MgH_2. Besides, $Mg(OH)_2$ does not form before pH 8.4.

Owing to hydrogen generation, the local pH at the interfaces of matrix and electrolyte would be promoted causing alkalization effect, prompting the formation of $Mg(OH)_2$. According to Song et al. [42, 43], the anodic dissolution of magnesium is a transient process,

Figure 7: Proposed Pourbaix diagram for Mg in water [41].

which is related to the formation of monovalent magnesium ion. However, monovalent magnesium ion has not been detected by any electrochemical method. Besides, there has been no thermodynamic data of the formation of monovalent magnesium ion [41]. According to Perrault [44], the Gibbs energies of the formation of Mg^{2+}, MgH_2, and $Mg(OH)_2$ are all below zero, implying their spontaneous formation processes. Furthermore, Mg cannot effectively hold hydrogen in its interior structure [41], leading to hydrogen release from its structure begins and therefore, such formation of MgH_2 does not require development of the unipositive Mg^+ ion as an intermediate in the corrosion of Mg. Moreover, when the hydrogen over-potential is high enough, formation rate of magnesium hydride is greater than the decomposition rate, and partial magnesium hydride becomes one of corrosion products left on the surface. It must be noted that hydride developed at interior of matrix by the reaction of hydrogen and matrix is stable (Eq. 2) [41]:

$$Mg + 2H_{ad} \rightarrow MgH_2 \qquad (2)$$
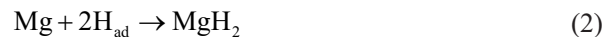
The presence of this composition was also confirmed by SIMS in situ observation [41, 45]. MgH_2 can be developed on the whole range of pH; however it decomposes into hydroxide and hydrogen gas when contacting water, according to Eq. 3 [41]:

$$MgH_2 + 2H_2O \rightarrow Mg(OH)_2 + 2H_2 \uparrow \qquad (3)$$
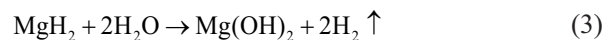
Yao et al. [46] reported that the film on pure Mg formed in 3% NaCl solution is more hydrated than that formed in distilled water. The hydration of the

Yeganeh M & Saremi M

Int. J. Bio-Inorg. Hybr. Nanomater., Vol. 3, No. 3 (2014), 135-142

oxides causes the conversion of the cubic oxide to hexagonal magnesium hydroxide with twice volume of the original oxide, resulting in a considerable disruption of the film [47]. The main role of the Cl^- anions in film breakdown has been attributed to the formation of soluble magnesium hydroxy-chloride complexes. It has been demonstrated that the solubility product (Ksp) of $Mg(OH)_2$ increases with chloride ion concentration. Investigation of the film formed on the Mg surface revealed presence of magnesium chlorides and hydroxy-chlorides within the $Mg(OH)_2$ layer, indicating that incorporation of Cl^- is a precursor to film breakdown. Therefore, breakdown occurs at a weak point in the surface film, where Cl^- migration causes an increase in the solubility of $Mg(OH)_2$ [48, 49].

At final times of corrosion (B: pH = 11.2, OCP = -1.39 vs. SCE), the presence of $Mg(OH)_2$ on the surface is emphasized by Pourbaix diagram. Here, an increase in OCP towards positive direction is a sign of development of more protective compound such as $Mg(OH)_2$.Therefore, it is expected that corrosion mechanism as well as inductive loop at the initial times (pH<8.4) is not attributed to $Mg(OH)_2$ formation. Thus, it can be postulated that the formation of inductive loop in the low frequency region could be attributed to several processes at these times. Development of such a loop can be attributed to formation of MgH_2 and $Mg(OH)_2$ at the initial and final times, respectively. In addition, the presence of chloride ion could introduce some pits on $Mg(OH)_2$ surface.

4. CONCLUSIONS

In this article biocompatible mesoporous silica was used as a host for corrosion inhibitor for Mg. These particles were embedded in the Alkyd resin and applied on the Mg surface. Then corrosion properties of Mg were compared to those of Alkyd coating. Results showed that coating with mesoporous silica loaded by corrosion inhibitor has a higher corrosion resistance compared to Mg and Alkyd/MS. Moreover, the surface of Alkyd/MSInh after corrosion showed more intact surface in comparison with the other samples.

REFERENCES

1. Staiger M.P., Pietak AM., Huadmai J., Dias G., *Biomater.*, **27** (2006), 1728.
2. Walker J.,Shadanbaz S.,Woodfield T.B.F., Staiger M.P., Dias G., *J. Biomed. Mater. Res. Part B*, 2014, In Press.
3. Xin Y., Liu C., Zhang X., Tang G., Tian X., Chub P.K., *J. Mater. Res.*, **22** (2007), 2004.
4. Hollstein F., Wiedemann R., Scholz J., *Surf. Coating. Technol.*, **162** (2003), 261.
5. Altun H., Sen S., *Surf. Coating. Technol.*, **174** (2003), 1018.
6. Song Y.W., Shan D.Y., Han E.H., *Electrochim. Acta*, **53** (2008), 2135.
7. Zhao H.,Huang Z., Cui J., *J. Mater. Process. Technol.*, **203** (2008), 310.
8. Ma Y., Nie X., Northwood D.O., Hu H., *Thin. Solid. Film*, **494** (2006), 296.
9. Duan H., Yan C., Wang F., *Electrochim. Acta*, **52** (2007), 3785.
10. Rudd A.L., Breslin C.B., Mansfeld F., *Corros. Sci.*, **42** (2000), 275.
11. Dabala M., Brunelli K., Napolitani E., Magrini M., *Surf. Coating Technol.*, **172** (2003), 227.
12. Chong K.Z., Shih T.S., *Mater. Chem. Phys.*, **80** (2003), 191.
13. Tan A.L.K., Soutar A.M., Annergren I.F., Liu Y.N., *Surf. Coating Technol.*, **198** (2005), 478.
14. Lamaka S.V., Montemor M.F., Galio A.F., Zheludkevich M.L., Trindade C., Dick L.F., Ferreira M.G.S., *Electrochim. Acta*, **53** (2008), 4773.
15. Tamar Y., Mandler D., *Electrochim. Acta*, **53** (2008), 5118.
16. Xu L., Pan F., Yu G., Yang L., Zhang E., Yang K., *Biomater.*, **30** (2009), 1512.
17. Shadanbaz S., Dias G.J., *Acta Biomater.*, **8** (2012), 20.
18. Song Y.W., Shan D.Y., Han E.H., *Mater. Lett.*, **62**

(2008), 3276.

19. Hiromoto S., Yamamoto A., *Electrochim. Acta*, **54** (2009), 7085.

20. Masanari T., Hiromoto S., *Appl. Surf. Sci.*, **257** (2011), 8253.

21. Truong V.T., Lai P.K., Moore B.T., Muscat R.F., Russo M.S., *Synth. Metal.*, **110** (2000), 7.

22. Wong H.M., Yeung K.W.K., Lam K.O., Tam V., Chu P.K., Luk K.D.K., Cheung K.M.C., *Biomater.*, **31** (2010), 2084.

23. Hu R.G., Zhang S., Bu J.F., Lin C.J., Song G.L., *Prog. Org. Coating*, **73** (2012), 129.

24. Walcarius A., *Chem. Soc. Rev.*, **42** (2013), 4098.

25. Wu S.H., Mou C.Y., Lin H.P., *Chem. Soc. Rev.*, **42** (2013), 3862.

26. Tarn D., Ashley C.E., Xue M., Carnes E.C., Zink J.I., Brinker C.J., *Acc. Chem. Res.*, **46** (2013), 792.

27. Pebere N., Riera C., Dabosi F., *Electrochim. Acta*, **35** (1990), 555.

28. Song G., Atrens A., StJohn D., Wu X., Nairn J., *Corros. Sci.*, **39** (1997), 1981.

29. Baril G., Pebere N., *Corros. Sci.*, **43** (2001), 471.

30. Metikos-Hukovic M., Babic R., Grubac Z., Brinic S., *J Appl. Electrochem.*, **24** (1994), 772.

31. Zhang Y., Yan C., Wang F., Li W., *Corros. Sci.*, **47** (2005), 2816.

32. Alvarez-Lopez M., Pereda M.D., Valle J.A., Fernandez-Lorenzo M., Garcia-Alonso M.C., Ruano O.A., Escudero M.L., *Acta Biomater.*, **6** (2010), 1763.

33. Arrabal R., Matykina E., Viejo F., Skeldon P., Thompson G.E., *Corros. Sci.*, **50** (2008), 1744.

34. Ying-liang C., Ting-wei Q., Hui-min W., Zhao Z., *Trans. Nonferrous Met. Soc. China.*, **19** (2009), 517.

35. Li Z., Song G.L., Song S., *Electrochim. Acta*, **115** (2014), 56.

36. Balbo A., Frignani A.,Grassi V., Zucchi F., *Corros. Sci.*, **73** (2013), 80.

37. Bastos A.C., Ferreira M.G.S., Simoes A.M.P., *Corros. Sci.*, **69** (2013),87.

38. LebriniM., LagreneeM., Vezin H., Traisnel M., Bentiss F., *Corros. Sci.*, **49** (2007), 2254.

39. King A.D., Birbilis N., Scully J.R., *Electrochim. Acta*, **121** (2014), 394.

40. Mahdavian M., Attar M.M., *Corros. Sci.*, **48** (2006), 4152.

41. Chen J., Dong J., Wang J., Han E., Ke W., *Corros. Sci.*, **50** (2008), 3610.

42. Song G.L., AtrensA., *Adv. Eng. Mater.*, **1** (1999), 11.

43. Song G., Atrens A., *Adv. Eng. Mater.*, **5** (2003), 837.

44. Perrault G., *J. Electroanal. Chem. Inter. Electrochem.*, **25** (1974), 107.

45. Chen J., WangJ., Han E., Dong J., Ke W., *Corros. Sci.*, **50** (2008), 1292.

46. Yao H.B., Li Y.,Wee A.T.S., *Appl. Surf. Sci.*, **158** (2000), 112.

47. Wu G., Fan Y., Atrens A., Zhai C., Ding W., *J. Appl. Electrochem.*, **38** (2008),251.

48. Williams G., McMurray H.N., *J. Electrochemi. Soc.*, **155** (2008), C340.

49. Wang L., Zhang B.P., Shinohara T., *Mater. Des.*, **31** (2010), 857.